Loss of Function of *RIMS2* Causes a Syndromic Congenital Cone-Rod Synaptic Disease with Neurodevelopmental and Pancreatic Involvement

Sabrina Mechaussier,[1,19] Basamat Almoallem,[2,3,19] Christina Zeitz,[4] Kristof Van Schil,[2] Laila Jeddawi,[5] Jo Van Dorpe,[6] Alfredo Dueñas Rey,[2] Christel Condroyer,[4] Olivier Pelle,[7] Michel Polak,[8] Nathalie Boddaert,[9] Nadia Bahi-Buisson,[10] Mara Cavallin,[11] Jean-Louis Bacquet,[12] Alexandra Mouallem-Bézière,[12] Olivia Zambrowski,[12,13] José Alain Sahel,[4,14,15,16,17] Isabelle Audo,[4,14,18,20] Josseline Kaplan,[1,12,20] Jean-Michel Rozet,[1,20] Elfride De Baere,[2,21,*] and Isabelle Perrault[1,21,*]

Congenital cone-rod synaptic disorder (CRSD), also known as incomplete congenital stationary night blindness (iCSNB), is a non-progressive inherited retinal disease (IRD) characterized by night blindness, photophobia, and nystagmus, and distinctive electroretinographic features. Here, we report bi-allelic *RIMS2* variants in seven CRSD-affected individuals from four unrelated families. Apart from CRSD, neurodevelopmental disease was observed in all affected individuals, and abnormal glucose homeostasis was observed in the eldest affected individual. RIMS2 regulates synaptic membrane exocytosis. Data mining of human adult bulk and single-cell retinal transcriptional datasets revealed predominant expression in rod photoreceptors, and immunostaining demonstrated RIMS2 localization in the human retinal outer plexiform layer, Purkinje cells, and pancreatic islets. Additionally, nonsense variants were shown to result in truncated RIMS2 and decreased insulin secretion in mammalian cells. The identification of a syndromic stationary congenital IRD has a major impact on the differential diagnosis of syndromic congenital IRD, which has previously been exclusively linked with degenerative IRD.

Introduction

Retinal rod and cone cells are photosensitive neurons that possess ribbon synapses to provide rapid and sustained transmission of graded light responses to second-order neuron bipolar and horizontal cells that shape the visual message for the cortex.[1] Genetic alterations affecting synaptic transmission from photoreceptors to bipolar cells manifest in congenital stationary night blindness (CSNB [MIM: PS310500]). It is a rare but also overlooked retinal disorder with an estimated prevalence of at least 1:40,000 (according to data drawn from a French cohort that included individuals confirmed to have the disease). This form of CSNB can be subdivided in complete (cCSNB) and incomplete (iCSNB) forms.[2] Whereas cCSNB affects mainly proteins located

post-synaptically at the dendritic tips of on-center bipolar cells (ON-bipolar cells), which are active when the light is on, iCSNB affects mainly proteins located at the synapse of photoreceptor cells.[2] Affected individuals with iCSNB are characterized by the dysfunction of both off-center bipolar cells (OFF-bipolar), which are active when the light is off, and ON-bipolar cells as shown in the electroretinogram (ERG).[2] Pathogenic variants in *CACNA1F* (MIM: 300110),[3,4] *CABP4* (MIM: 608965),[5] and *CACNA2D4* (MIM: 608171)[6] were identified in affected individuals with iCSNB.[2] Of note, in addition to the fact that phenotypic variability can lead to mildly progressive inherited retinal disorders (IRDs), stable low vision, nystagmus, and more importantly, photophobia might also be major symptoms in affected individuals with variants in *CACNA1F*, *CABP4*, and *CACNA2D4*,[2]

[1]Laboratory of Genetics in Ophthalmology, INSERM UMR 1163, Institute of Genetic Diseases, Imagine and Paris University, 75015 Paris, France; [2]Center for Medical Genetics and Department of Biomolecular Medicine, Ghent University and Ghent University Hospital, 9000 Ghent, Belgium; [3]Department of Ophthalmology, King Abdul-Aziz University Hospital, College of Medicine, King Saud University, Riyadh, Saudi Arabia; [4]Sorbonne Université, INSERM, Centre National de la Recherche Scientifique, Institut de la Vision, 75012 Paris, France; [5]Pediatric Ophthalmology Division, Dhahran Eye Specialist Hospital, Dhahran 34257, Saudi Arabia; [6]Department of Pathology, Ghent University and Ghent University Hospital, 9000 Ghent, Belgium; [7]Cell Sorting Facility, INSERM UMR 1163, Institute of Genetic Diseases, Imagine and Paris University, 75015 Paris, France; [8]Endocrinology, Gynecology, and Pediatric Diabetology Department, University Hospital Necker-Enfants Malades, Assistance Publique-Hôpitaux de Paris, 75015 Paris, France; [9]Department of Pediatric Radiology, University Hospital Necker-Enfants Malades, Assistance Publique-Hôpitaux de Paris, 75015 Paris, France; [10]Pediatric Neurology Department, University Hospital Necker-Enfants Malades, Assistance Publique-Hôpitaux de Paris, 75015 Paris, France; [11]Laboratory of Embryology and Genetics of Human Malformation, INSERM UMR 1163, Institute of Genetic Diseases, Imagine and Paris University, 75015 Paris, France; [12]Service d'Ophtalmologie, Centre Hospitalier Intercommunal de Créteil, Assistance Publique-Hôpitaux de Paris, 94000 Créteil, France; [13]Ophthalmology Department, University Hospital Necker-Enfants Malades, Assistance Publique-Hôpitaux de Paris, 75015 Paris, France; [14]Centre Hospitalier National d'Ophtalmologie des Quinze-Vingts, INSERM, Direction de l'Hospitalisation et de l'Organisation des Soins (DHOS), Centres d'Investigations Cliniques (CIC) 1423, 75012 Paris, France; [15]Fondation Ophtalmologique Adolphe de Rothschild, 75019 Paris, France; [16]Académie des Sciences, Institut de France, 75006 Paris, France; [17]Department of Ophthalmology, The University of Pittsburgh School of Medicine, Pittsburgh, Pennsylvania, PA 15213, USA; [18]Institute of Ophthalmology, University College of London, London EC1V 9EL, UK

[19]These authors contributed equally to this work
[20]These authors contributed equally to this work
[21]These authors contributed equally to this work

*Correspondence: isabelle.perrault@inserm.fr (I.P.), elfride.debaere@ugent.be (E.D.B.)

and thus, the term iCSNB might be misleading.[7,8] Therefore, we use the term congenital cone-rod synaptic disorder (CRSD).

The ocular presentation in infants might be reminiscent of Leber congenital amaurosis (LCA [MIM: PS204000]), a degenerative retinal disease that is a leading cause of childhood blindness; it has an estimated prevalence of 1:30,000.[9] Occasionally, LCA can be the earliest manifestation of syndromic disease, such as ciliopathies,[10] neuro-metabolic disorders,[11] or tubulinopathies.[12] ERG is a critical test for early differential diagnosis. ERG responses are undetectable, in keeping with the extremely severe rod and cone dysfunction in LCA. However in CRSD, ERG traces reveal generalized inner retinal dysfunction with both ON- and OFF-bipolar cell dysfunction: normal photoreceptor function manifests with an electronegative waveform in response to a bright flash under dark adaptation and with severely reduced and delayed light-adapted responses. However, ERG recordings might be challenging in young children, and this might contribute to a misdiagnosis of the ultra-rare CRSD as the more prevalent LCA.

Here, a genomic study of individuals with IRD but an unresolved diagnosis revealed bi-allelic loss-of-function variants in regulating synaptic membrane exocytosis 2 (RIMS2 [MIM: 606630]) in seven affected individuals with an initial diagnosis of CSNB or LCA and who were from four unrelated families of Senegalese, French, and Saudi-Arabian origin. Consistent with a role of RIMS2 in regulating synaptic membrane exocytosis in the brain, pancreas, and photoreceptors and with its localization in human tissues, we demonstrated syndromic CRSD with neurodevelopmental and possible pancreatic involvement in individuals with bi-allelic mutations in RIMS2.

Materials and Methods

Subjects
This study involved seven affected subjects (three females and four males) with early-onset IRD and five healthy relatives from four unrelated families. Families 1 and 2 were studied at Imagine-Necker-Enfants Malades University Hospital. Affected individual III-3 of family 1 (F1:III-3 in Figure 1A) was also studied at the Centre Hospitalier National d'Ophtalmologie des Quinze-Vingts. Family 3 was clinically studied at the Pediatric Ophthalmology Division at the Dhahran Eye Specialist Hospital in Dhahran, Saudi Arabia, and Family 4 was studied at the Centre Hospitalier National d'Ophtalmologie des Quinze-Vingts. Family 1, referred for LCA, has an inbred Senegalese pedigree with several consanguinity loops and three affected individuals over two generations (two adult sisters and the child of one of them; the child was born to a first-cousin marriage). Family 2, referred for LCA, comprises a single affected individual and his two unrelated parents of French origin. Family 3 includes an affected sibship born to a first-cousin marriage and is from Saudi Arabia. Family 4, with a clinical diagnosis of CSNB, consists of a single affected individual originating from first-degree cousins; the mother is Franco-Senegalese, and the father is of Senegalese descent (Figure 1A). All individuals or legal representatives consented with the study, which received approval from the institutional review boards Comité de Protection des Personnes Ile de France II (Necker), Ile de France V (project number 06693, EudraCT number 2006-A00347-44, 11 December 2006, Quinze-Vingts), and Ghent University Hospital Ethics Committee (B670201734438). Genomic DNA was extracted from peripheral blood by standard procedures.

Genetic Analysis
The notation of the variants was based on RIMS2α transcript GenBank: NM_00134848.1, corresponding to the variant X5 transcript for GenBank: XM_033203201 (version XM_033203201.1).

Gene-Panel Testing and Exome Sequencing
Families 1 and 2 underwent testing with a small IRD panel followed by exome sequencing (ES). Genomic DNA libraries were generated from DNA (F1:III-3, F1:III-5, F2:I-1, F2:I-2, and F2:II-2) sheared with a Covaris S2 Ultrasonicator via SureSelect[XT] Library Prep Kit (Agilent). Regions of interest (ROIs) were captured with the SureSelect All Exon V5 kit (Agilent) and sequenced on an Illumina HiSeq2500 HT system (Illumina). Data analysis was performed with a homemade pipeline (POLYWEB)[13] created by the Imagine Institute Bioinformatics core facilities of Paris Descartes University.

Whole-Genome Homozygosity Mapping and ES
DNA from F3:II-1 and F3:II-2 of family 3 were genotyped with the HumanCytoSNP-12 BeadChip platform (Illumina). The genotypes were evaluated for runs of homozygosity (ROH) >1 Mb via PLINK software[14] integrated in in-house software ViVar.[15] Resulting ROH were ranked according to their length and number of consecutive homozygous single-nucleotide polymorphisms (SNPs).[16] For ES, exome enrichment and sequencing were performed with the Agilent SureSelect Human All exon V5/V6 kit followed by paired-end sequencing on a HiSeq2000 (2 × 100 cycles). The CLC Genomics Workbench version 9.0.1 (CLCBio) was used for read-mapping against the human genome reference (NCBI build37/hg19 version), post-mapping duplicate read removal, coverage analysis, and quality-based variant calling via Alamut (visual version 2.7.2; interactive biosoftware).

Targeted Testing of RIMS2
Forty-six affected individuals diagnosed with iCSNB and 133 affected individuals diagnosed with LCA underwent RIMS2 testing either by Sanger sequencing (Big Dye Terminator v3.1 Kit, Applied Biosystems) or targeted next-generation sequencing (Nextera XT DNA Library Prep kit, MiSeq, Illumina) (Tables S1A and S1B). We confirmed RIMS2 variants identified by ES, and we performed segregation analysis by Sanger sequencing in all available family members (Figure 1A).

RIMS2 Expression Studies in Human Tissues
Data Mining in Human Adult Single-Cell Retinal Transcriptional Datasets
Data was processed for evaluating RIMS2 expression at the single-cell (sc) level. The expression matrix derived from pooling three donor neural retina samples[17] was retrieved and imported into R (v.3.6.2) with the Seurat sc analysis package (v3.1.4).[18] We conducted pre-processing and quality control to remove outlier cells. We filtered out cells that had unique (gene) feature counts less than 200 or greater than 2,500 and that expressed >5% mitochondrial counts. The dataset was subsequently normalized via the built-in global-scaling normalization method "LogNormalize."
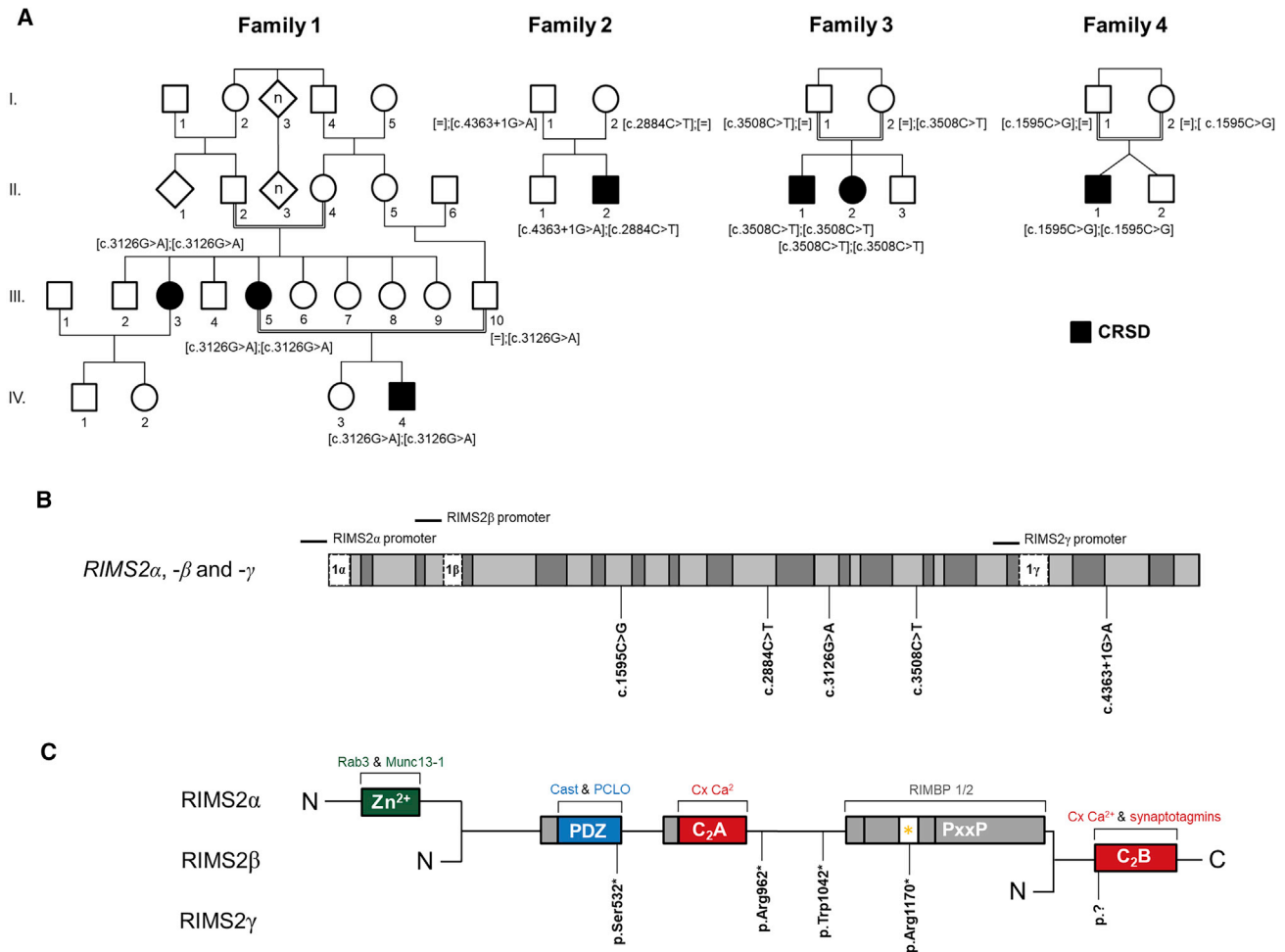
Figure 1. Bi-allelic *RIMS2α* Variants in the Four Families and Location in RIMS2α, RIMS2β, and RIMS2γ Isoforms and Domain Structure

(A) Pedigrees of families and segregation analysis of the variants. Positions of c.3126G>A (p.Trp1042*), c.2884C>T (p.Arg962*), c.4363+1G>A (p.?), c.3508C>T (p.Arg1170*), and c.1595C>G (p.Ser532*) substitutions corresponding to *RIMS2α*. The WT allele is represented by an equal sign.

(B) Diagram of the human *RIMS2* showing positions of the c.1595C>G, c.2884C>T, c.3126G>A, c.3508C>T, and c.4363+1G>A variants. *RIMS2α*, GenBank: NM_00134848.1 (GRCh38). *RIMS2β*, GenBank: NM_001348494.1 (GRCh38). *RIMS2γ*, GenBank: NM_001282882.1 (GRCh38). The positions of specific *RIMS2α*, -*β*, and -*γ* promoters are located above the diagram.

(C) Diagram showing predicted protein domains in the three isoforms RIMS2α, RIMS2β, and RIMS3γ; the positions of p.Ser532*, p.Arg962*, p.Trp1042*, p.Arg1170*, and p.? variants correspond to the RIMS2α isoform. Abbreviations used: Zn^{2+}, N-terminal zinc finger domain; PDZ, central PDZ domain; C_2A and C_2B, central and C-terminal C2 domains, respectively; PxxP, proline-rich sequence; asterisk, SH3 domain-binding motif.

Prior to dimensional reduction, the data was subjected to scaling, and heterogeneity associated with the number of unique molecular identifiers (UMIs) per cell and mitochondrial contamination was regressed out. After quality control pre-processing, a total of 15,635 cells were kept and clustered via the K-nearest neighbor graph method implemented in Seurat after PCA-reduction. We applied the non-linear dimensional reduction technique UMAP (uniform manifold approximation and projection)[19] to visualize and explore the dataset. As input, the same principal components from the clustering analysis were used. We used markers associated with major neural retina cell populations to assess *RIMS2* expression at the sc level.

Data Mining in Human Adult Bulk Retinal Transcriptional Datasets
Expression levels in terms of transcripts per million (TPM) were retrieved from postmortem retina samples characterized in Ratnap-

riya et al.[20] A total of 453 samples that passed quality control were considered first. In order to avoid introducing confounding variables in the downstream analysis, we selected only donor retinas without age-related macular degeneration, resulting in 105 individual samples. For gene set selection, TPM values were further filtered for a set of candidate genes, which included all genes reported to cause IRD (RetNet) and genes identified in synaptic vesicle pools and/or with pre- and post-synaptic-curated annotations (SynGO).[21] A total of 379 genes were eventually considered. For normalization, stabilization, and statistics, prior to examining correlations in the expression of the candidate genes, the set was further filtered by both mean expression and variance. To remove potential noise, we first filtered out the 25% of genes with the lowest mean expression across all samples. We then subjected the set to a variance-stabilizing transformation to correct for

mean-variance dependency;[22,23] this resulted in a total of 289 genes' being retained. We then examined the expression of *RIMS2* and several synaptic genes (*CACNA1F, CABP4, CACNA2D4,* and *SV2B*). For each gene pair, Spearman's correlations were computed along with pairwise p values adjusted for multiple comparisons (Holm's method). A matrix correlation plot was then generated for visualization.

Expression Analysis
RT-qPCR was performed with the total RNA of fetal brain (22 weeks), retina (16 weeks), and head of the pancreas (25 weeks) (RNeasy Mini Kit, QIAGEN), and for cDNA synthesis, random hexamer anchored oligo(dT) primers were used (Verso cDNA Kit, Life Technologies Thermo Fisher Scientific). We measured *RIMS2* expression by amplifying 138, 78, and 89 bp fragments (Table S1C). Real-time PCR amplification and normalization were performed as described.[24] Data were analyzed with Realplex software (Eppendorf).

Immunohistochemistry
Human retinal, brain, and pancreatic tissues used for immunohistochemistry were fixed in 10% neutral buffered formaldehyde and embedded in paraffin. Staining for RIMS2 was performed on 3-μm-thick sections via an automatic immunostainer (BenchMark Ultra, Ventana Medical Systems). The rabbit polyclonal antibody anti-RIMS2 (1:25; Antibodies-Online: ABIN1003091) was used, and visualization was achieved with the OptiView Amplification Kit (Ventana Medical Systems). Heat-induced epitope retrieval was performed with Cell Conditioning 2 (Ventana Medical Systems).

Functional Analysis of *RIMS2* Nonsense Variants

Site-Directed Mutagenesis
Constructs were made for the following variants: c.1595C>G, c.2884C>T, c.3126G>A, and c.3508C>T. We did this by using mutagenesis via inverse PCR with Phusion polymerase and by using vector pcDNA3.1/(+)-N-(K)-DYK-RIMS2α (RIMS2α, NM: 00134848.1; 10,277 bp) (Genscript) as a template. Primers can be found in Table S1D. We digested the amplified product with *Dpn*I to avoid re-ligation of the original non-mutated DNA. We amplified constructs in TOP10 Chemically Competent *Escherichia coli* cells, and we sequenced inserts to assess the mutagenesis and the rest of the sequence.

Immunoblot Analysis in HEK293 Cells
5×10^5 cells/well in 6-well plates were co-transfected with wild-type (WT) or mutant FLAG-tagged RIMS2 plasmids (1.6 μg; Genscript) and the pCAGGS-GFP plasmid (400 ng; Clontech) with the FuGene HD transfection reagent according to the manufacturer's protocol (Promega). Proteins were prepared with radioimmunoprecipitation assay (RIPA) lysis buffer (Life Technologies Thermo Fisher Scientific). 50 μg of total proteins were resolved by Mini-ProteanTGX Stain Free 4%–15% gel according to the recommendations of the supplier (BioRad). Proteins were transferred to a polyvinylidene fluoride (PVDF) membrane via an RTA Transfer Kit (BioRad), and the membrane was probed with the following primary antibodies: polyclonal goat IgG anti-DDDDK tag (1:5,000; Abcam) and monoclonal mouse IgG1κ anti-GFP (1:2,000; Sigma Aldrich). Rabbit anti-goat IgG-HRP (1:2,000; Abcam) and rabbit anti-mouse IgG-HRP (1:2,000; Abcam) were used as secondary antibodies. Blots were developed with the Clarity Western ECL and ChemiDoc XRS+ Imaging System (BioRad). Immunoblot images were acquired and analyzed via Image Lab Software 3.0.1 build 18 (BioRad). The abundance of FLAG relative to GFP was estimated by densitometry with the Image Lab Software 3.0.1 build 18. A Student's t test was performed.

Insulin Secretion Assay in MIN6B1 Cells
Clone B1 derived from Mouse insulinoma pancreatic 6 β-cells (MIN6 B1) were seeded at 3×10^6 cells/well in 6-well plates and co-transfected with WT or mutant FLAG-tagged RIMS2 plasmids (2 μg, Genscript) and the pCAGGS-GFP plasmid (1 μg; Clontech) via the FuGene HD transfection reagent according to the manufacturer's protocol (Promega). GFP-expressing cells from cell pools were sorted on a BD FACSAria II (BD Biosciences) with special order research products (SORP) program. GFP-MIN6 B1 cells were seeded at 5×10^4 cells/well in 96-well plates. After 1 h of DMEM Glutamax I medium (5 mM glucose), the medium was replaced by DMEM Glutamax I medium (25 mM glucose). Concentration of insulin in the medium was determined with the Insulin Mouse ELISA Kit (Invitrogen Thermo Fisher Scientific) after 25 min of incubation. Absorbance was measured immediately at 450 nm and 550 nm by a VICTOR X4 2030 multilabel plate reader (Perki-nElmer). Using Prism6 software, we determined the significance of variations among samples via a one-way ANOVA with a post hoc Tukey's test.

Results

Identification of Bi-allelic *RIMS2* Variants in Seven Cases from Four Unrelated Families
Exome datasets were generated for affected siblings F1:III-3 and F1:III-5 and F3:II-1 and F3:II-2 and for affected individual F2:II-2 and his unaffected parents, F2:I-1 and F2:I-2 (Figure 1A). By applying stringent filtering, we found a total of seven and two candidate genes in family 1 and family 2, respectively (Table S2). This strategy revealed bi-allelic *RIMS2* variants (GenBank: XM_033203201) in the two families: c.3126G>A (p.Trp1042*) in F1:III-3 and F1:III-5 (homozygous) and c.2884C>T (p.Arg962*) in *trans* with c.4363+1G>A (p.?) in F2:II-2. Similarly, homozygosity mapping combined with ES in family 3 identified a homozygous *RIMS2* variant, c.3508C>T (p.Arg1170*), in the largest 25 Mb autozygous region in F3:II-1 and F3:II-2 as the most plausible candidate variant (Table S2). Of note, no LOD score could be calculated as a result of the small size of the family. Subsequent targeted *RIMS2* testing of pre-screened affected individuals with iCSNB identified two affected individuals with a homozygous *RIMS2* variant: c.1595C>G (p.Ser532*) in F4:II-1 and c.3126G>A (p.Trp1042*) in an affected individual that retrospectively appeared to be related to family 1 (F1:III-3) (Figures 1B and 1C). Co-segregation of the *RIMS2* variants with the disease was confirmed (Figure 1A).

Clinical Re-evaluation of Affected Individuals
The complete lack of *Rims2* in the mouse has been reported to cause behavioral anomalies, defective synaptic visual signal transmission from photoreceptors to second-order retinal neurons consistent with iCSNB, and insulin resistance.[25] In family 1, the affected individual F1:III-5 and her elder, affected sister F1:III-3 were born to consanguineous parents from Senegal and were reported to have manifested nystagmus, poor visual function, and altered ERGs around birth. Upon ophthalmological evaluation, the
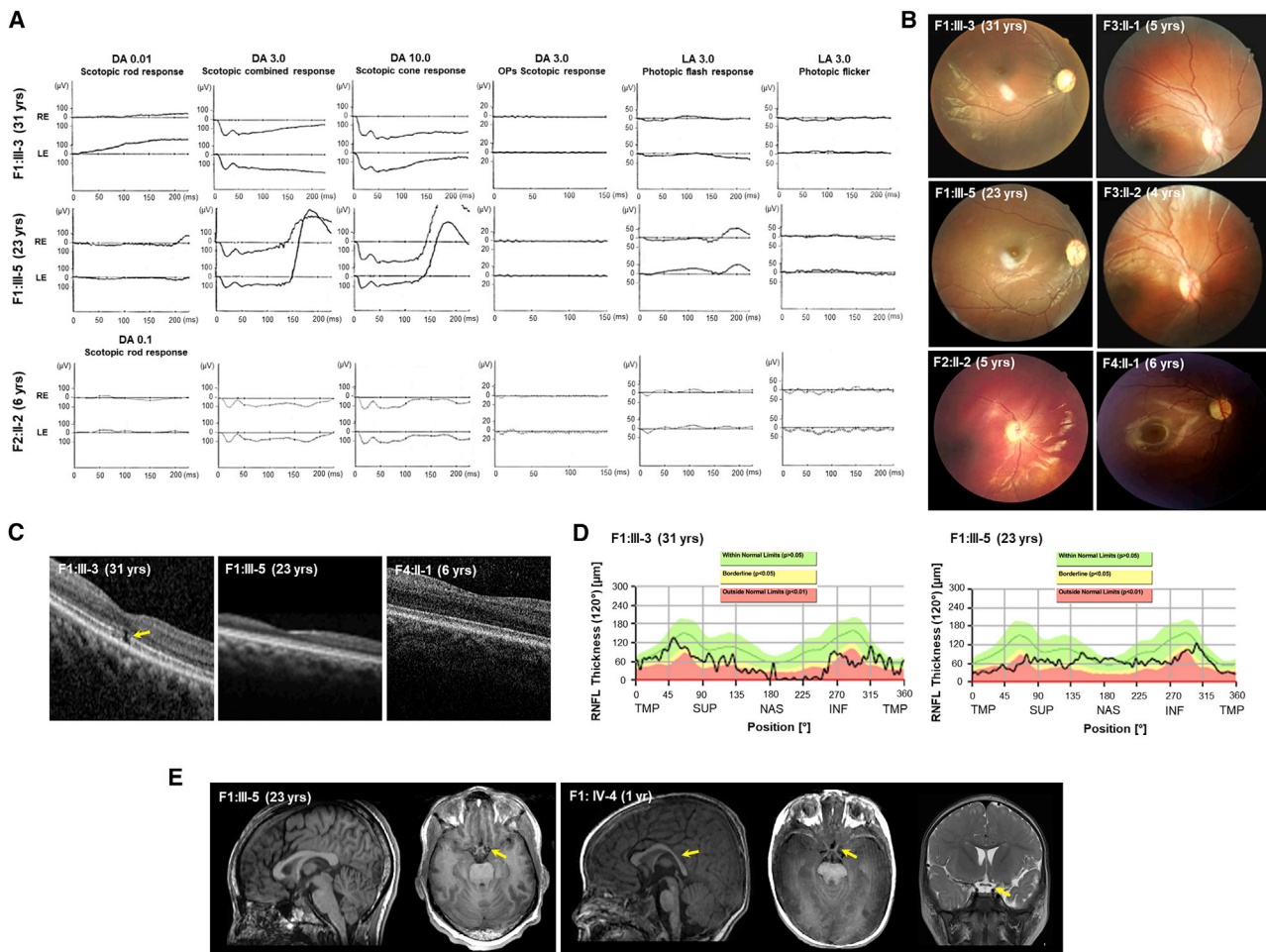
Figure 2. Clinical Presentation of Affected Individuals

(A) Representative ERG in affected individuals F1:III-3 and F1:III-5 carrying the homozygous c.3126G>A (p.Trp1042*) *RIMS2* variant and in affected individual F2:II-2 who is compound heterozygous with c.2884C>T (p.Arg962*) and c.4363+1G>A (p.?) *RIMS2* variants.

(B) Color fundus photographs of the right eye of affected individuals F1:III-3, F1:III-5, F2:II-2, F3:II-1, F3:II-2, and F4:II-1.

(C) Horizontal scan of macular spectral-domain optic-coherence tomography (macular SD-OCT) from the right eye of affected individuals F1:III-3, F1:III-5, and F4:II-1. Anomaly is marked by a yellow arrow.

(D) Representative spectral-domain optical coherence tomography of the area surrounding the optic nerve with measure of the retinal nerve fiber layer thickness (RNFL-SD-OCT) in affected individuals F1:III-3 and F1:III-5. Abbreviations used: TMP, temporal; SUP, superior; NAS, nasal; INF, inferior.

(E) Representative MRI in affected individuals F1:III-5 and F1:IV-4. MRI, magnetic resonance imaging. Anomalies are marked by yellow arrows.

sisters, currently aged 23 and 31 years and having had myopic correction, displayed features of inner retinal dysfunction: in response to a bright flash under dark-adapted conditions such features included a preserved a-wave (originating from photoreceptor hyperpolarization) but a severely reduced b-wave (originating from ON-bipolar depolarization) and severely reduced and delayed light-adapted responses, in keeping with cone ON- and OFF-bipolar cell dysfunction (Figure 2A). Funduscopy showed optic disc pallor, moderate vascular attenuation, normal macular area, and a normal mid-peripheral and peripheral aspect with no pigmentary migration (Figure 2B). Spectral-domain optical coherence tomography (SD-OCT) of the macular region revealed inner retinal thinning throughout the posterior pole and a disruption of the foveal ellipsoid line in F1:III-5 (Figure 2C), and SD-OCT

of the retinal nerve fiber layer (RNFL) revealed a temporal RNFL loss (Figure 2D). These data are consistent with a cone-rod synaptic disorder with additional foveal changes. Disc pallor, inner retinal changes, and thinned retinal vessels have to be interpreted in the context of high myopia. The eldest sister (F1:III-3) had a known history of persistent elevated blood glucose since the age of 29 years, and fasting blood glucose testing confirmed the diagnosis of insulin-dependent diabetes mellitus (Table 1). Clinical neurologic assessment and neuroimaging of the youngest affected sister, F1:III-5, demonstrated autistic features with unremarkable cerebral anomalies with the exception of temporal optic-nerve atrophy. She displayed marked lipoatrophy with facial sparing, but the metabolic workup was unremarkable; in particular, there was no resistance to insulin and no alteration of blood-glucose homeostasis.

Table 1. Summary of Clinical Features of Seven Affected Individuals from Four Families with *RIMS2* Variants

Individual	F1:III-3	F1:III-5	F1:IV-4	F2:II-2	F3:II-1	F3:II-2	F4:II-1
Age (years)	33	25	2	7	7	6	9
Origin	Senegal	Senegal	Senegal	France	Saudi Arabia	Saudi Arabia	France/Senegal
Ophthalmologic Features							
Nystagmus	+	+	erratic ocular movement	erratic ocular movement	+	+	+
Photophobia	+	+	+	+	+	+	+
Night blindness	−	−	−	−	−	−	+
Visual acuity (RE)	20/250	20/3200	NP	20/320	LP	LP	around 20/200
Visual acuity (LE)	20/320	20/320	NP	20/320	LP	LP	around 20/200
Refractive error (RE)	−2 (1.75) 90°	−0.75 (1.25) 20°	+2.25	+6	NA	NA	−3 (−1) 175°
Refractive error (LE)	−1	−2.50 (−2.25) 170°	+3	+6	NA	NA	−4.50 (−2) 170°
ERG electronegativity	present	present	NP	present	NP	NP	present
Fundus	optic disc pallor; no peripheral pigmentary migration, greyish retina	temporal optic disc pallor; no peripheral pigmentary migration	temporal optic disc pallor; no peripheral pigmentary migration	optic disc pallor; no peripheral pigmentary migration	temporal optic-disc pallor; no peripheral pigmentary migration	temporal optic-disc pallor; no peripheral pigmentary migration	temporal optic-disc pallor; no peripheral pigmentary migration
Macular SD-OCT	retinal thinning at the expense of inner retina	retinal thinning at the expense of inner retina; retrofoveal focal ellipsoid zone disruption	NP	retinal thinning at the expense of inner retina	NA	NA	normal
RNFL-SD-OCT	NA (optic nerve dysversion)	temporal RNFL loss	NP	NP	NA	NA	NA
Autofluorescence	normal	normal	NP	normal	NA	NA	normal
Neurologic Features							
Neurological examination	NP	autistic behavior	neuro developmental delay; general movement disorganization; ataxia manifestations; poor language	autistic features: stereotypies/OCD	severe autistic behavior; aggressivity; anxiety; no language	autistic behavior; poor language	neuro developmental delay, eventually with no learning disability; ataxia; hyperactive and mild autistic behavior; delay in language acquisition
MRI	normal	normal	dysmorphic corpus callosum	normal	NA	NA	normal
Metabolic Features							
Fasting blood glucose	insulin-dependent diabetes mellitus	normal: 0.94 g/L	NP	normal: 0.85 g/L	NP	NP	NP
Blood glucose	hyperglycemia: 1.26 g/L	hyperglycemia: 1.13 g/L	hyperglycemia: 1.33 g/L	NP	NP	NP	normal

Ophthalmologic, neurologic, and metabolic investigations in all affected individuals. Abbreviations used: CF, count fingers; LP, light perception; ERG, electroretinogram; RE, right eye; LE, left eye; BE, both eyes; SD-OCT, spectral-domain optical-coherence tomography; RNFL-SD-OCT, spectral-domain optical-coherence tomography measuring the retinal nerve fiber layer thickness; MRI, magnetic resonance imaging; OCD, obsessive-compulsive disorders; NA, not available; NP, not performed.

Lipid homeostasis and liver function were also not altered. Her affected son, F1:IV-4, was born to a first-cousin marriage and presented at 13 months of age with severe visual dysfunction and marked neurodevelopmental delay (poor language, mild ataxia, general movement disorganization) with a dysmorphic corpus callosum at brain magnetic resonance imaging (MRI; Figure 2E). The metabolic workup was unremarkable (Table 1). The young individual IV-4 in family 1 was born to a double-consanguineous marriage. Because the familial *RIMS2* pathogenic variant in IV-4 was found by targeted *RIMS2* testing and not by whole-exome sequencing (WES), we cannot rule out the possibility that dysmorphology of the corpus callosum is attributed to a homozygous pathogenic variant in another gene because of this parental consanguinity.

Affected individual F2:II-2 was born at term after an uneventful pregnancy. He was first seen in ophthalmology at 2.5 months for pendular nystagmus, strabismus, and photophobia. Upon examination, he presented with hyperopia, the inability to follow lights or objects, and a normal fundus. At the age of 7 months, the poor quality of ERG recording led to a presumed diagnosis of LCA. At 2 years of age, the child manifested behavioral problems and an inability to walk without assistance. In addition to nystagmus and photophobia, the ophthalmologist noted some albinoid characteristics, including fair ashy hairs, peripheral iris transillumination, and pale fundus. Furthermore, bilateral active pupillary reflexes were present, calling the initial ERG results and diagnosis of LCA into question. However, ERG recordings could not be repeated at that time because of high agitation. Genotype-directed clinical reexamination was conducted at the age of 5.5–6 years. ERG recordings under general anesthesia revealed an electronegative waveform under limited dark adaptation and barely detectable photopic responses, consistent with iCSNB (Figure 2A). Funduscopy showed optic nerve pallor and a normal mid-peripheral and peripheral aspect (Figure 2B). Neuropediatric assessment showed autistic features, including stereotypies and obsessive-compulsive disorder (OCD). Neuroimaging with MRI displayed no brain anomalies. The blood-glucose homeostasis dosage was in the normal range (Table 1).

The two affected sibling of family 3 (F3:II-1 and F3:II-2) were born to consanguineous Saudi Arabian parents and displayed poor visual acuity reaching light perception in both eyes, photophobia, pendular nystagmus, the absence of pupillary response, and oculo-digital signs. Retinal imaging of both siblings showed a waxy pallor of the optic discs and attenuated retinal vessels (Figure 2B). Both siblings displayed autistic behavior with a variable degree of severity: whereas the female younger sibling, F3:II-2 (3 years), could produce simple speech, the male sibling, F3:II-1 (4 years), was not capable of speech and showed aggressive and anxious behavior (Table 1), thus not allowing for ERG recordings.

Affected individual F4:II-1 of family 4 was born to consanguineous Senegalese parents. He was first referred to the electrophysiology unit when he was 2.5 years of age for photophobia, nystagmus, and poor vision. He was a premature (born at 33 weeks after amenorrhea) twin baby, and his fraternal twin brother was exempt of any relevant medical and ophthalmic history besides the prematurity and a mild ataxia that developed while he was starting to walk at 14 months of age. F4:II-1 had been diagnosed with developmental delay with delayed speech and walking; these delays were resolving upon rehabilitation. After thorough psychomotor examination, a diagnosis of attention disorder with hyperactivity within the spectrum of autistic behavior was diagnosed; he had no intellectual disability. His metabolic work-up was otherwise normal. F3:II-1 was myopic and had a visual acuity around 20/200 for both eyes at age 7 years (Table 1). Fundus examination revealed a mild optic-disc pallor and some vessel attenuation that could be attributed to the myopia (Figure 2B). SD-OCT of the macula was normal (Figure 2C). Fundus autofluorescence was normal. ERG recordings revealed an electronegative waveform to a bright flash in dark-adapted conditions as well as delayed and reduced responses in light adaptation, leading to a diagnosis of iCSNB. The child manifested neurodevelopmental delay with speech difficulties but no learning disability in elementary school, an ataxic gait, and a certain degree of hyperactive autistic behavior (Table 1).

RIMS2 Is Present in the Human Retina, Brain, and Pancreas

Consistent with the neuro-ophthalmo-metabolic phenotype of the knock-out model, *Rims2* is detected in mouse retinal, brain, and pancreatic tissues (see BioGPS in Web Resources). According to the human retinal transcriptome dataset of the Ocular Genomics Institute, the Human Protein Atlas, and BioGPS, human RIMS2 is equally detected in these tissues. Data mining of sc transcriptional datasets of human adult neural retina showed that *RIMS2* was predominantly expressed in rod photoreceptor clusters (Figure S1A) and has an expression pattern similar to that of *CABP4* (Figure S1B). Next, we assessed the expression patterns of *RIMS2*, *CACNA1F*, *CABP4*, *CACNA2D4*, and *SV2B* in human adult bulk retinal transcriptional datasets for coordinated correlation, reasoning that this could provide insight into potential regulatory interactions. A matrix correlation plot (Figure S1C) showed *RIMS2* expression to be anti-correlated with *CACNA1F* (rho = −0.3435, p = 0.002) and to be correlated with *SV2B* (rho = 0.6565, p < 0.0001). The latter is known to be localized in synaptic vesicles, where it might function in the regulation of vesicle trafficking and exocytosis.

In addition to a promoter located in the 5′ UTR region driving the longest *RIMS2α* transcript, the gene has two internal alternative promoters yielding shorter transcripts (*RIMS2β* and *RIMS2γ*) (Figure 1B). RT-qPCR analysis with primers specific for each of the three isoforms applied to fetal human tissues showed that all transcripts were expressed far more highly in the brain than in other tissues.
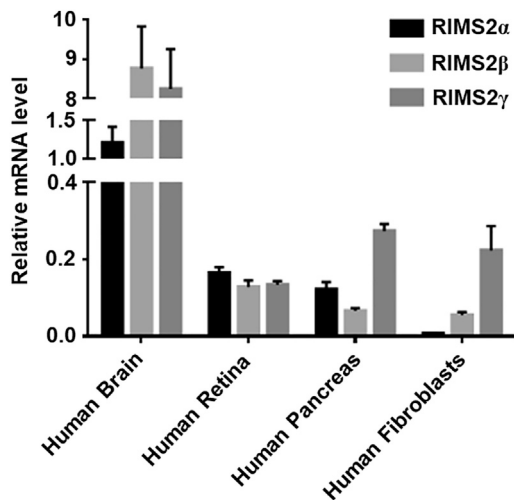
Figure 3. Expression Analysis of *RIMS2* mRNA in Fetal Human Tissues by Quantitative Real-Time PCR
Quantitative expression analysis in fetal human tissues. Error bars reflect the standard errors of the mean (SEMs).

In the retina, the three transcripts seemed equally expressed. In the pancreas, *RIMS2γ* had the highest expression, followed by *RIMS2α* then *RIMS2β,* whereas *RIMS2α* expression was undetectable in fibroblasts; these non-neuronal, non-secretory cells showed predominant *RIMS2γ* expression (Figure 3).

We assessed RIMS2 localization in adult human retina, brain, and pancreas by immunostaining using an antibody recognizing both RIMS2α and RIMS2β isoforms but not RIMS2γ. Strong and specific RIMS2 immunostaining was observed in the outer plexiform retinal layer (Figure 4A), cerebellar cortical neurons (more specifically in Purkinje cells; Figure 4B), and pancreatic Langerhans islets (Figure 4C). This localization is in agreement with the spectrum of oculo-cerebro-pancreatic anomalies in individuals with bi-allelic mutant *RIMS2* variants.

In Silico Predictions and *In Vitro* Functional Characterization of *RIMS2* Variants
Effect of a Splice Variant
The c.4363+1G>A splice variant found in family 2 is the only one out of five unique *RIMS2* variants that is expected to affect the three transcripts. *In silico* predictions suggest the presence of an abolished consensus donor splice-site leading to the skipping of the adjacent exon, a frameshift, and the introduction of a premature termination codon (c.4251_4363del [p.Asn1417Lysfs*2]). The insertion of a stop codon in the shortest *RIMS2γ* transcript most likely results in nonsense-mediated decay (NMD) and in the absence of this an isoform. The mutant *RIMS2α* and *RIMS2β* transcripts, however, might escape NMD and lead to truncated isoforms (Figure S2).

Protein Abundance of Nonsense Variants
The four *RIMS2* nonsense variants, however, are predicted to produce normal RIMS2γ and truncated RIMS2α and RIMS2β. Consistent with this, immunoblot analysis using

FLAG antibody of lysates from HEK293 cells overexpressing individually the WT, p.Ser532*, p.Arg962*, p.Trp1042*, and p.Arg1170* FLAG-tagged *RIMS2α* cDNAs revealed an ~210 kDa protein and truncated isoforms of expected ~60, ~120, ~130, and ~150 kDa sizes, respectively (Figure 5A). The WT and truncated FLAG-tagged proteins were produced with the same intensity (Figure 5B). When using the primary antibodies polyclonal rabbit IgG anti-RIMS2 (1:1000; Synaptic Systems Cat. No. 140 303) and monoclonal mouse IgG anti-β-actin (1:4000; Abcam) and the secondary antibodies goat anti-rabbit IgG-HRP (1:2000; Abcam) and goat anti-mouse IgG-HRP (1:2000; Abcam), we detected no endogenous RIMS2α or RIMS2β in lysates from untransfected HEK293 cells (Figure S3).

Insulin Secretion in MIN6B1 Cells
We investigated the ability of these truncated proteins that lack all or most of the domain that interacts with RIM-binding proteins 1 and 2 (RIMBP1 and RIMBP2) to promote insulin secretion in MIN6B1 cells. We overexpressed the pCAGGS-GFP plasmid alone or in combination with the WT or mutant FLAG-tagged RIMS2 constructs and measured the accumulation of insulin in the culture medium upon glucose stimulation. The amount of insulin in the culture medium from cells transfected with pCAGGS-GFP alone was in the same range as that in medium from cells transfected with pCAGGS-GFP in combination with the WT FLAG-tagged RIMS2α constructs, suggesting that overexpression of WT RIMS2α does not affect insulin secretion. In contrast, we observed a reproducible reduction of insulin accumulation in cells transfected with each of the three mutant constructs, supporting that truncation of all or most of the RIMBP1- and RIMBP2-binding domain alters insulin secretion in this cellular system (Figure 6).

Discussion

The human visual system continues to develop after birth, mainly in the first years of life. The differential diagnosis of early-onset IRD, either stationary (CSNB) or degenerative (LCA), might be challenging in the first months of life, mainly as a result of individuals' inability to respond verbally to visual testing, the absence of apparent fundus changes, the difficulties in cooperation for testing, especially in individuals with behavioral problems that might lead to unreliable ERG recordings, and the presence of a nystagmus, all of which, without general anesthesia, hamper high-resolution retinal imaging. The identification of the underlying genetic defect can accelerate an early differential diagnosis between a stationary and degenerative retinal disease because there is no genetic overlap.

Here, we demonstrated the bi-allelic loss of function of *RIMS2* in a phenotype characterized by syndromic CRSD with neurodevelopmental and pancreatic involvement, consistent with a role of RIMS2 in regulating synaptic
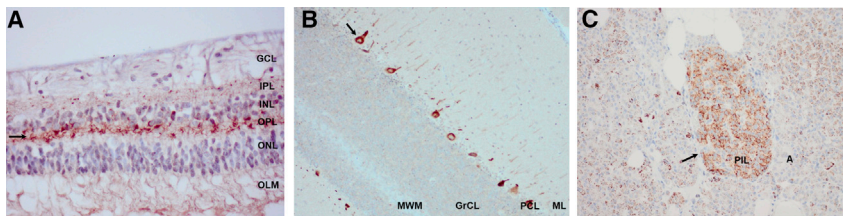
Figure 4. Immunohistochemistry of RIMS2 in the Adult Human Brain, Pancreas, and Retina

(A–C) Immunostaining of RIMS2 protein is indicated in brown and showed by the arrows in the retina (A), the brain (B), and the pancreas (C). A specific RIMS2 antibody targets a region of the RIMS2α form (Antibodies-Online: ABIN1003091). Abbreviations used: GCL, ganglion cell layer; IPL, inner plexiform layer; INL, inner nuclear layer; OPL, outer plexiform layer; ONL, outer nuclear layer; OLM, outer limiting membrane; MWM, medulla of white matter; GrCL, granule cell layer; PCL, Purkinje cell layer; ML, molecular layer; PIL, pancreatic islet of Langerhans; A, acinus.

membrane exocytosis in the brain, pancreas, and photoreceptors. In regard to the retinal phenotype, visual acuity seems low in our individuals with *RIMS2*-associated CRSD and would be on the lower functional spectrum of the high phenotypic variability spectrum of iCSNB, which is characterized by a post-photoreceptor defect affecting both the cone and rod signaling pathways.[2] Indeed, in a series of 60 affected individuals carrying mutation in *CACNA1F*, Boycott et al. report a high variability in visual acuity in correlation with the presence of a nystagmus.[26] In addition, for some of the affected individuals in our study, behavioral disturbances made it difficult for us to accurately measure visual acuity, which as a result, might have been underestimated. Additionally, one of the affected individuals presented here had foveal changes that might have also hampered visual acuity. Similar changes have been reported in association with *CABP4* mutations.[27] These changes were only present once in our report, and further studies are needed to document the frequency of this occurrence in *RIMS2*-associated CRSD. Furthermore, one instance of inner retinal thinning was also found in our series, and such thinning might also contribute to poor visual acuity. This finding has also been reported in association with iCSNB.[28]

RIMS2 is one of the Rab3-interacting molecules, or RIMs, which are multi-domain scaffolding proteins that were first described as putative presynaptic active-zone proteins that play an essential role in neurotransmitter release and are located in the retinal photoreceptors.[29–31] In vertebrates, RIMs are encoded by four regulating synaptic membrane exocytosis genes (*RIMS1–RIMS4*).[30] Although *Rims1α*$^{-/-}$ and *Rims2α*$^{-/-}$ mice are viable, the ablation of both genes causes postnatal mortality as a result of a defective neurotransmitter release despite preserved synaptic structure and exocytosis ability.[32,33] Synapses of double mutants contain active zones and release neurotransmitters, but they cannot mediate normal Ca^{2+}-triggered release.[32,33] The *RIMS2*-associated phenotype in affected human individuals is consistent with the known function of the mouse ortholog in the photoreceptor ribbon synapse, conventional chemical synapse, and synaptic-vesicle exocytosis and with its localization in the outer retinal plexiform layer,[25] brain synapses,[32] and pancreatic β cells.[34]

RIMS2 is the predominant large RIM isoform present at photoreceptor ribbon synapses. RIMS2 plays an important role in maintaining the normal synaptic connection at the ribbon synapse of the photoreceptors.[1,25] This can be achieved via several interactions required for synaptic vesicle docking and priming.[29] The majority of photoreceptor RIMS2 lacks the N-terminal zinc finger and part of the RAB3A-binding domain, suggesting that photoreceptor synaptic transmission does not depend on full-length *RIMSα*.[25] The role of RIMS2 at photoreceptor ribbon synapses is different from RIM function in most other types of chemical synapses.[35] At the photoreceptor ribbon synaptic active zone, RIMS2 is not essential for vesicle priming[25] or Ca^{2+} channel clustering, but it does act as a Ca^{2+} channel modulator.[36] We assessed the influence of Rims1 and Rims2 on synaptic processes at rod terminals by generating a conditional double-knockout mouse model in rod photoreceptors at as early as 3 weeks of age. Deletion of *Rims1* and *Rims2* in mouse rods (called *Rims1/2* double knockout) showed a dramatic loss of Ca^{2+} influx through Cav1.4 channels and an associated reduction in evoked release.[36] Both Rims isoforms were shown to be expressed in the retina at as early as 3 weeks of age. However, it has been shown that the Rims1-specific antibody supports an absence of Rims1 from photoreceptors and their ribbon synapses in the outer plexiform layer and that Rims1α does not contribute to the regulation of exocytosis at the cone photoreceptor ribbon synapse.[25] 5 weeks later at 8 weeks, Rims2 was shown to be present exclusively in the outer plexiform layer of WT mice, whereas it was absent in the knockout mice. It was concluded that Rims2 potently enhances the influx of Ca^{2+}, which is vitally important for the release of vesicles from the rod ribbon possibly through direct or indirect modulation of the Cav1.4 channels.[36–38] As Rims2 has many partners that have not been linked with any human or animal phenotype so far at the photoreceptor synapse (synthesized in Figure 7),[1,29,35,37–43] the genes encoding them merit consideration in genomic studies of children with congenital IRD.

In regard to the brain, Rims2, like Rims1, was shown to be expressed at as early as 3 weeks of age in whole brain lysates. Analysis of double knockout mice has demonstrated expression of the two paralogs in overlapping but distinct patterns throughout the brain.[32,33] Here, we showed localization of RIMS2 in human adult cerebellar cortical neurons, more specifically in Purkinje cells. Of interest,
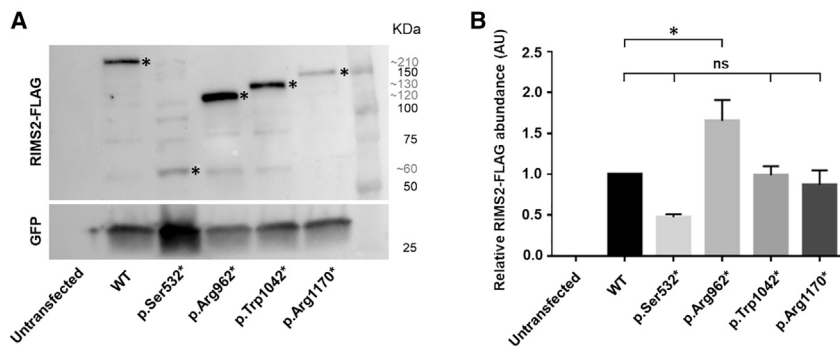
Figure 5. Immunoblot Analysis of HEK293 Cells Overexpressing WT and Mutant RIMS2

(A) Anti-RIMS2-FLAG antibody used to reveal only exogenous protein production in HEK293 cells. Anti-GFP antibody was used as a control condition. The WT condition corresponds to an overexpression of WT RIMS2 in HEK293 cells. The p.Ser532*, p.Arg962*, p.Trp1042*, and p.Arg1170* conditions correspond to an overexpression of mutant RIMS2 in HEK293 cells. Expected size bands are marked by dark stars.

(B) Relative quantification of RIMS2-FLAG proteins in HEK293 cells by the measurement of FLAG proteins compared to GFP proteins. Error bars reflect the standard errors of the mean (SEMs). *, p value < 0.5; ns, non-significant p value ≥ 0.5.

involvement of *RIMS2* in neurological disease, more specifically in autism spectrum disease (ASD), is supported by a genome-wide association study in affected individuals with Asperger syndrome (ASPG [MIM: 608638]), revealing a significant association with the *RIMS2*-associated SNP rs2080610.[44] A study on alternative splicing in neural tissues showed that one of the *RIMS2* transcripts contains a highly-conserved micro-exon that is neuron-specific.[45] *RIMS2* has been listed as an ASD-associated gene in a recently developed ASD database.[46]

Interestingly, a *RIMS1* variant was found to co-segregate with autosomal-dominant cone-rod dystrophy (CORD7 [MIM: 603649]) in a British family, implicating a gene with a synaptic function in an IRD.[47–49] In a mouse model carrying the same *Rims1* variant as the human CORD7 (p.Arg655His), the mutant was shown to modify Rims1 function in regulating voltage dependent Ca^{2+} channel currents.[50] A *Rims1* variant on different presynaptic voltage-dependent calcium channels (VDCCs) might eventually lead to CORD and enhanced cognitive abilities. Moreover, *RIMS1* has been associated with ASD by two independent studies.[51,52] Regarding *RIMS2*, a copy-number variant (CNV), more specifically a duplication of 277 kb (Chr8: 104901578–105178819), was found in an individual affected with autosomal-dominant retinitis pigmentosa (adRP [MIM: 268000]). Although this CNV was found to be absent in genomic databases, the role of this duplication in the pathogenesis of adRP is still a matter of debate, especially because no segregation analysis could be performed in the rest of the family, including the affected father.[53]

RIMS2 or *RIMS1* variants have not been associated with metabolic dysfunction before. Yet, RIMS2 has been identified by a yeast two-hybrid screen performed on pancreatic β cells to determine docking and priming states in insulin granule exocytosis.[34] Consistently, *Rims2*−/− mice display a phenotype that consists of anomalies of photoreceptor synaptic transmission,[25] deficit in maternal behavior,[32,33] and insulin resistance.[34] This retino-neuro-metabolic phenotype is reminiscent of the *RIMS2*-associated disease we report here. Whether abnormal glucose homeostasis

is an invariable feature remains to be confirmed. Evidence of insulin resistance in the eldest affected individual of our cohort suggests that this could be an age-related feature, and it will be important to perform a close follow-up of metabolic functions.

In summary, bi-allelic loss-of-function variants of *RIMS2* have been shown to cause a previously unreported syndromic iCSNB, manifesting as a CRSD with neurodevelopmental disease and occasional anomalies of glucose homeostasis. The identification of a syndromic stationary congenital IRD has a major impact on the differential diagnosis of syndromic congenital IRD, which has previously been exclusively linked with degenerative IRD. Finally, our study implicates a photoreceptor synaptic gene in syndromic disease.
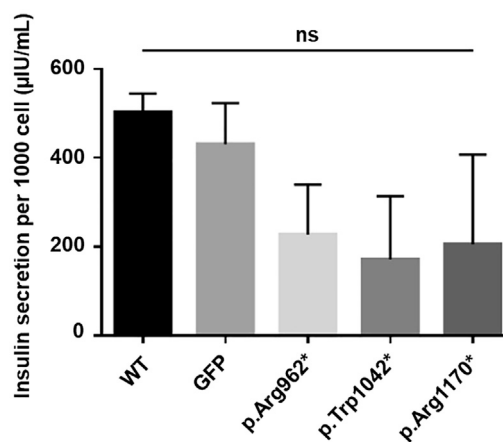

Figure 6. Insulin Secretion of MIN6 B1 Cells Overexpressing WT and Mutant RIMS2 After 25 min of Incubation with Glucose 25 mM

The WT condition corresponds to an overexpression of WT RIMS2 in MIN6 B1 cells. The GFP condition corresponds to an overexpression of GFP as a basal expression reporter of RIMS2 in MIN6 B1 cells. The p.Arg962* (c.2884C>T), p.Trp1042* (c.3126G>A), and p.Arg1170* (c.3508C>T) conditions correspond to an overexpression of mutant RIMS2 in MIN6 B1 cells. Insulin secretion is measured at 25 min after the supply of glucose in medium cells by ELISA. Error bars reflect the standard errors for the mean (SEMs). ns, non-significant p value ≥ 0.5.
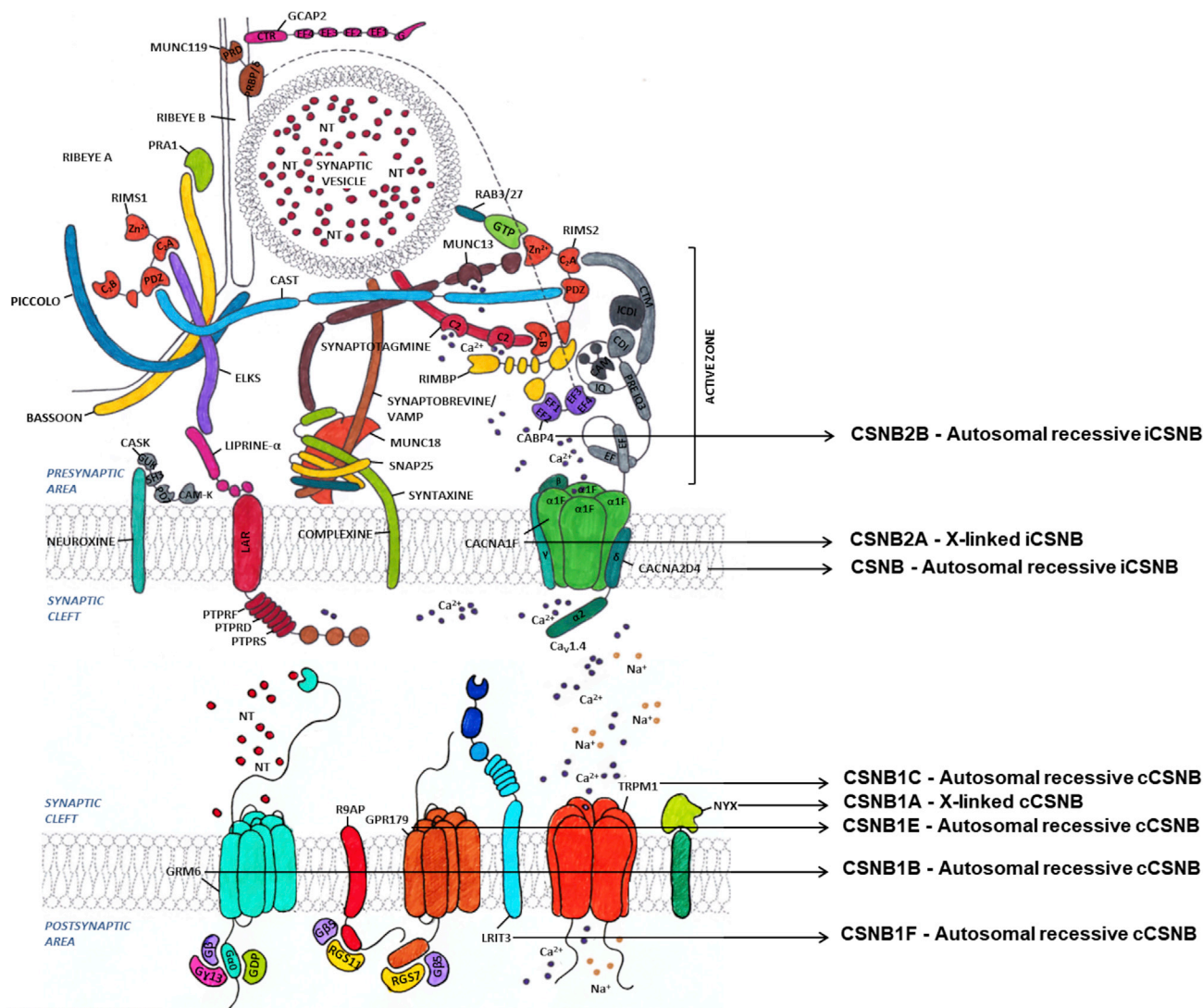
Figure 7. Schematic and Simplified Drawing of Protein Complexes Present at the Photoreceptor Ribbon Synapses
Presynaptic photoreceptor, synaptic cleft, and postsynaptic bipolar areas are shown. The names of proteins are indicated after dashes. The names of protein domains are directly indicated on the protein drawing. Proteins that have already been implicated in CSNB are indicated with an arrow. Abbreviations used: NT, neurotransmitters; iCSNB, incomplete form of congenital stationary night blindness; cCSNB, complete form of congenital stationary night blindness; Ca^{2+}, calcium; Na^+, sodium.

Supplemental Data

Supplemental Data can be found online at https://doi.org/10.1016/j.ajhg.2020.04.018.

Acknowledgments

Centre Hospitalier National d'Ophtalmologie des Quinze-Vingts, INSERM, and CNRS). E.D.B., C.Z., I.A., J.-A.S., and J.-M.R. are members of the European Reference Network for Rare Eye Diseases (ERN-EYE), which is co-funded by the Health Program of the European Union under the Framework Partnership Agreement 739534.

Declaration of Interests

The authors declare no competing interests.

Web Resources

BioGPS, biogps.org/
Ocular Genomics Institute, https://oculargenomics.meei.harvard.edu/
OMIM, https://omim.org/
RetNet, https://sph.uth.edu/retnet/
The Human Protein Atlas, www.proteinatlas.org/

References

1. Mercer, A.J., and Thoreson, W.B. (2011). The dynamic architecture of photoreceptor ribbon synapses: cytoskeletal, extracellular matrix, and intramembrane proteins. Vis. Neurosci. 28, 453–471.

2. Zeitz, C., Robson, A.G., and Audo, I. (2015). Congenital stationary night blindness: an analysis and update of genotype-phenotype correlations and pathogenic mechanisms. Prog. Retin. Eye Res. 45, 58–110.

3. Strom, T.M., Nyakatura, G., Apfelstedt-Sylla, E., Hellebrand, H., Lorenz, B., Weber, B.H., Wutz, K., Gutwillinger, N., Rüther, K., Drescher, B., et al. (1998). An L-type calcium-channel gene mutated in incomplete X-linked congenital stationary night blindness. Nat. Genet. 19, 260–263.

4. Bech-Hansen, N.T., Naylor, M.J., Maybaum, T.A., Pearce, W.G., Koop, B., Fishman, G.A., Mets, M., Musarella, M.A., and Boycott, K.M. (1998). Loss-of-function mutations in a calcium-channel α1-subunit gene in Xp11.23 cause incomplete X-linked congenital stationary night blindness. Nat. Genet. 19, 264–267.

5. Zeitz, C., Kloeckener-Gruissem, B., Forster, U., Kohl, S., Magyar, I., Wissinger, B., Mátyás, G., Borruat, F.X., Schorderet, D.F., Zrenner, E., et al. (2006). Mutations in CABP4, the gene encoding the Ca2+-binding protein 4, cause autosomal recessive night blindness. Am. J. Hum. Genet. 79, 657–667.

6. Wycisk, K.A., Zeitz, C., Feil, S., Wittmer, M., Forster, U., Neidhardt, J., Wissinger, B., Zrenner, E., Wilke, R., Kohl, S., and Berger, W. (2006). Mutation in the auxiliary calcium-channel subunit CACNA2D4 causes autosomal recessive cone dystrophy. Am. J. Hum. Genet. 79, 973–977.

7. Khan, A.O. (2014). CABP4 mutations do not cause congenital stationary night blindness. Ophthalmology 121, e15.

8. Riemslag, F.C.C. (2009). Visually impaired children: "coming to better terms". Doc. Ophthalmol. 119, 1–7.

9. Kaplan, J. (2008). Leber congenital amaurosis: from darkness to spotlight. Ophthalmic Genet. 29, 92–98.

10. Waters, A.M., and Beales, P.L. (2011). Ciliopathies: an expanding disease spectrum. Pediatr. Nephrol. 26, 1039–1056.

11. Casteels, I., Spileers, W., Demaerel, P., Casaer, P., De Cock, P., Dralands, L., and Missotten, L. (1996). Leber congenital amaurosis–differential diagnosis, ophthalmological and neuroradiological report of 18 patients. Neuropediatrics 27, 189–193.

12. Luscan, R., Mechaussier, S., Paul, A., Tian, G., Gérard, X., Defoort-Dellhemmes, S., Loundon, N., Audo, I., Bonnin, S., LeGargasson, J.F., et al. (2017). Mutations in TUBB4B cause a distinctive sensorineural disease. Am. J. Hum. Genet. 101, 1006–1012.

13. Gerber, S., Alzayady, K.J., Burglen, L., Brémond-Gignac, D., Marchesin, V., Roche, O., Rio, M., Funalot, B., Calmon, R., Durr, A., et al. (2016). Recessive and dominant de novo ITPR1 mutations cause gillespie syndrome. Am. J. Hum. Genet. 98, 971–980.

14. Purcell, S., Neale, B., Todd-Brown, K., Thomas, L., Ferreira, M.A., Bender, D., Maller, J., Sklar, P., de Bakker, P.I., Daly, M.J., and Sham, P.C. (2007). PLINK: a tool set for whole-genome association and population-based linkage analyses. Am. J. Hum. Genet. 81, 559–575.

15. Sante, T., Vergult, S., Volders, P.J., Kloosterman, W.P., Trooskens, G., De Preter, K., Dheedene, A., Speleman, F., De Meyer, T., and Menten, B. (2014). ViVar: a comprehensive platform for the analysis and visualization of structural genomic variation. PLoS ONE 9, e113800.

16. Coppieters, F., Van Schil, K., Bauwens, M., Verdin, H., De Jaegher, A., Syx, D., Sante, T., Lefever, S., Abdelmoula, N.B., Depasse, F., et al. (2014). Identity-by-descent-guided mutation analysis and exome sequencing in consanguineous families reveals unusual clinical and molecular findings in retinal dystrophy. Genet. Med. 16, 671–680.

17. Lukowski, S.W., Lo, C.Y., Sharov, A.A., Nguyen, Q., Fang, L., Hung, S.S., Zhu, L., Zhang, T., Grünert, U., Nguyen, T., et al. (2019). A single-cell transcriptome atlas of the adult human retina. EMBO J. 38, e100811.

18. Satija, R., Farrell, J.A., Gennert, D., Schier, A.F., and Regev, A. (2015). Spatial reconstruction of single-cell gene expression data. Nat. Biotechnol. 33, 495–502.

19. Becht, E., McInnes, L., Healy, J., Dutertre, C.A., Kwok, I.W.H., Ng, L.G., Ginhoux, F., and Newell, E.W. (2018). Dimensionality reduction for visualizing single-cell data using UMAP. Nat. Biotechnol. 37, 38–44.

20. Ratnapriya, R., Sosina, O.A., Starostik, M.R., Kwicklis, M., Kapphahn, R.J., Fritsche, L.G., Walton, A., Arvanitis, M., Gieser, L., Pietraszkiewicz, A., et al. (2019). Retinal transcriptome and eQTL analyses identify genes associated with age-related macular degeneration. Nat. Genet. 51, 606–610.

21. Koopmans, F., van Nierop, P., Andres-Alonso, M., Byrnes, A., Cijsouw, T., Coba, M.P., Cornelisse, L.N., Farrell, R.J., Goldschmidt, H.L., Howrigan, D.P., et al. (2019). SynGO: an evidence-based, expert-curated knowledge base for the synapse. Neuron 103, 217–234.e4.

22. Russo, P.S.T., Ferreira, G.R., Cardozo, L.E., Bürger, M.C., Arias-Carrasco, R., Maruyama, S.R., Hirata, T.D.C., Lima, D.S., Passos, F.M., Fukutani, K.F., et al. (2018). CEMiTool: a Bioconductor package for performing comprehensive modular co-expression analyses. BMC Bioinformatics 19, 56.

23. Zwiener, I., Frisch, B., and Binder, H. (2014). Transforming RNA-Seq data to improve the performance of prognostic gene signatures. PLoS ONE 9, e85150.

24. Gerard, X., Perrault, I., Hanein, S., Silva, E., Bigot, K., Defoort-Delhemmes, S., Rio, M., Munnich, A., Scherman, D., Kaplan,

J., et al. (2012). AON-mediated Exon Skipping Restores Ciliation in Fibroblasts Harboring the Common Leber Congenital Amaurosis CEP290 Mutation. Mol. Ther. Nucleic Acids *1*, e29.

25. Löhner, M., Babai, N., Müller, T., Gierke, K., Atorf, J., Joachimsthaler, A., Peukert, A., Martens, H., Feigenspan, A., Kremers, J., et al. (2017). Analysis of RIM expression and function at mouse photoreceptor ribbon synapses. J. Neurosci. *37*, 7848–7863.

26. Boycott, K.M., Pearce, W.G., and Bech-Hansen, N.T. (2000). Clinical variability among patients with incomplete X-linked congenital stationary night blindness and a founder mutation in CACNA1F. Can. J. Ophthalmol. *35*, 204–213.

27. Smirnov, V.M., Zeitz, C., Soumittra, N., Audo, I., and Defoort-Dhellemmes, S. (2018). Retinal findings in a patient of French ancestry with CABP4-related retinal disease. Doc. Ophthalmol. *136*, 135–143.

28. Chen, R.W.S., Greenberg, J.P., Lazow, M.A., Ramachandran, R., Lima, L.H., Hwang, J.C., Schubert, C., Braunstein, A., Allikmets, R., and Tsang, S.H. (2012). Autofluorescence imaging and spectral-domain optical coherence tomography in incomplete congenital stationary night blindness and comparison with retinitis pigmentosa. Am. J. Ophthalmol. *153*, 143–54.e2.

29. Acuna, C., Liu, X., and Südhof, T.C. (2016). How to make an active zone: unexpected universal functional redundancy between RIMs and RIM-BPs. Neuron *91*, 792–807.

30. Wang, Y., and Südhof, T.C. (2003). Genomic definition of RIM proteins: evolutionary amplification of a family of synaptic regulatory proteins. Genomics *81*, 126–137.

31. Heidelberger, R., Thoreson, W.B., and Witkovsky, P. (2005). Synaptic transmission at retinal ribbon synapses. Prog. Retin. Eye Res. *24*, 682–720.

32. Schoch, S., Mittelstaedt, T., Kaeser, P.S., Padgett, D., Feldmann, N., Chevaleyre, V., Castillo, P.E., Hammer, R.E., Han, W., Schmitz, F., et al. (2006). Redundant functions of RIM1α and RIM2α in Ca(2+)-triggered neurotransmitter release. EMBO J. *25*, 5852–5863.

33. Schoch, S., Castillo, P.E., Jo, T., Mukherjee, K., Geppert, M., Wang, Y., Schmitz, F., Malenka, R.C., and Südhof, T.C. (2002). RIM1α forms a protein scaffold for regulating neurotransmitter release at the active zone. Nature *415*, 321–326.

34. Yasuda, T., Shibasaki, T., Minami, K., Takahashi, H., Mizoguchi, A., Uriu, Y., Numata, T., Mori, Y., Miyazaki, J., Miki, T., and Seino, S. (2010). Rim2α determines docking and priming states in insulin granule exocytosis. Cell Metab. *12*, 117–129.

35. Mittelstaedt, T., Alvaréz-Baron, E., and Schoch, S. (2010). RIM proteins and their role in synapse function. Biol. Chem. *391*, 599–606.

36. Grabner, C.P., Gandini, M.A., Rehak, R., Le, Y., Zamponi, G.W., and Schmitz, F. (2015). RIM1/2-mediated facilitation of Cav1.4 channel opening is required for Ca2+-stimulated release in mouse rod photoreceptors. J. Neurosci. *35*, 13133–13147.

37. Hibino, H., Pironkova, R., Onwumere, O., Vologodskaia, M., Hudspeth, A.J., and Lesage, F. (2002). RIM binding proteins (RBPs) couple Rab3-interacting molecules (RIMs) to voltage-gated Ca(2+) channels. Neuron *34*, 411–423.

38. Kaeser, P.S., Deng, L., Wang, Y., Dulubova, I., Liu, X., Rizo, J., and Südhof, T.C. (2011). RIM proteins tether Ca2+ channels to presynaptic active zones via a direct PDZ-domain interaction. Cell *144*, 282–295.

39. Schmitz, F., Natarajan, S., Venkatesan, J.K., Wahl, S., Schwarz, K., and Grabner, C.P. (2012). EF hand-mediated Ca- and cGMP-signaling in photoreceptor synaptic terminals. Front. Mol. Neurosci. *5*, 26.

40. tom Dieck, S., and Brandstätter, J.H. (2006). Ribbon synapses of the retina. Cell Tissue Res. *326*, 339–346.

41. tom Dieck, S., Altrock, W.D., Kessels, M.M., Qualmann, B., Regus, H., Brauner, D., Fejtová, A., Bracko, O., Gundelfinger, E.D., and Brandstätter, J.H. (2005). Molecular dissection of the photoreceptor ribbon synapse: physical interaction of Bassoon and RIBEYE is essential for the assembly of the ribbon complex. J. Cell Biol. *168*, 825–836.

42. Rizo, J. (2018). Mechanism of neurotransmitter release coming into focus. Protein Sci. *27*, 1364–1391.

43. Wahl-Schott, C., Baumann, L., Cuny, H., Eckert, C., Griessmeier, K., and Biel, M. (2006). Switching off calcium-dependent inactivation in L-type calcium channels by an autoinhibitory domain. Proc. Natl. Acad. Sci. USA *103*, 15657–15662.

44. Salyakina, D., Ma, D.Q., Jaworski, J.M., Konidari, I., Whitehead, P.L., Henson, R., Martinez, D., Robinson, J.L., Sacharow, S., Wright, H.H., et al. (2010). Variants in several genomic regions associated with asperger disorder. Autism Res. *3*, 303–310.

45. Irimia, M., Weatheritt, R.J., Ellis, J.D., Parikshak, N.N., Gonatopoulos-Pournatzis, T., Babor, M., Quesnel-Vallières, M., Tapial, J., Raj, B., O'Hanlon, D., et al. (2014). A highly conserved program of neuronal microexons is misregulated in autistic brains. Cell *159*, 1511–1523.

46. Krishnan, A., Zhang, R., Yao, V., Theesfeld, C.L., Wong, A.K., Tadych, A., Volfovsky, N., Packer, A., Lash, A., and Troyanskaya, O.G. (2016). Genome-wide prediction and functional characterization of the genetic basis of autism spectrum disorder. Nat. Neurosci. *19*, 1454–1462.

47. Kelsell, R.E., Gregory-Evans, K., Gregory-Evans, C.Y., Holder, G.E., Jay, M.R., Weber, B.H., Moore, A.T., Bird, A.C., and Hunt, D.M. (1998). Localization of a gene (CORD7) for a dominant cone-rod dystrophy to chromosome 6q. Am. J. Hum. Genet. *63*, 274–279.

48. Warwick, A.N., Shawkat, F., and Lotery, A.J. (2017). Retinitis pigmentosa and bilateral cystoid macular oedema in a patient heterozygous for the RIM1 mutation previously associated with cone-rod dystrophy 7. Ophthalmic Genet. *38*, 178–182.

49. Johnson, S., Halford, S., Morris, A.G., Patel, R.J., Wilkie, S.E., Hardcastle, A.J., Moore, A.T., Zhang, K., and Hunt, D.M. (2003). Genomic organisation and alternative splicing of human RIM1, a gene implicated in autosomal dominant cone-rod dystrophy (CORD7). Genomics *81*, 304–314.

50. Miki, T., Kiyonaka, S., Uriu, Y., De Waard, M., Wakamori, M., Beedle, A.M., Campbell, K.P., and Mori, Y. (2007). Mutation associated with an autosomal dominant cone-rod dystrophy CORD7 modifies RIM1-mediated modulation of voltage-dependent Ca2+ channels. Channels (Austin) *1*, 144–147.

51. Dong, S., Walker, M.F., Carriero, N.J., DiCola, M., Willsey, A.J., Ye, A.Y., Waqar, Z., Gonzalez, L.E., Overton, J.D., Frahm, S., et al. (2014). De novo insertions and deletions of predominantly paternal origin are associated with autism spectrum disorder. Cell Rep. *9*, 16–23.

52. Krumm, N., Turner, T.N., Baker, C., Vives, L., Mohajeri, K., Witherspoon, K., Raja, A., Coe, B.P., Stessman, H.A., He, Z.X., et al. (2015). Excess of rare, inherited truncating mutations in autism. Nat. Genet. *47*, 582–588.

53. Huang, X.-F., Mao, J.Y., Huang, Z.Q., Rao, F.Q., Cheng, F.F., Li, F.F., Wang, Q.F., and Jin, Z.B. (2017). Genome-wide detection of copy number variations in unsolved inherited retinal disease. Invest. Ophthalmol. Vis. Sci. *58*, 424–429.